2021 International Conference on Unmanned Aircraft Systems (ICUAS)
Athens, Greece. June 15-18, 2021

Velocity estimation for UAVs using ultra wide-band system

Ali Safaei
Dep. of Mechanical Engineering
McGill University
Montreal, Canada
ali.safaei@mail.mcgill.ca

Inna Sharf
Dep. of Mechanical Engineering
McGill University
Montreal, Canada
inna.sharf@mcgill.ca

2021 International Conference on Unmanned Aircraft Systems (ICUAS) | 978-1-6654-1535-4/21/$31.00 ©2021 IEEE | DOI: 10.1109/ICUAS51884.2021.9476831

***Abstract*—In this paper, a 3D velocity estimation solution based on ultra wide-band (UWB) signals is developed for navigation of unmanned aerial vehicles (UAVs) in indoor spaces. The solution incorporates two consecutive gradient descent optimizations for position and velocity estimation, as well as two linear Kalman filters for removing noise on the range measurements and the vertical position estimate. The solution is verified by three experimental scenarios with manual and autonomous flights of a quadrotor. In our implementation, 8 anchors are employed to construct the UWB system, while the Vicon MoCap system is utilized as the ground-truth for assessing the performance of the solution. All proposed algorithms are implemented on a computer on-board the quadrotor, with the low-level control for the quadrotor provided by the PX4 platform. Compared to a motion capture system, a relatively cheap solution for both absolute position and velocity estimation is achieved using the UWB system, with sufficient accuracy for autonomous flight of UAVs in indoor areas.**

I. Introduction

Ultra Wide Band (UWB) signal is a radio frequency signal, with a special feature of having a crisp pulse, compared to the narrow band signals available in WiFi, Bluetooth and ZigBee technologies. This feature makes UWB superior for determining the exact time of transmission and reception of the signal. It is an important feature for a ranging process—the process of distance estimation between a transmitter and a receiver based on the time of flight of a signal. Thus, majority of the indoor position estimation techniques available for the UWB modules are based on the estimation of time of flight for signals sent from multiple anchors (i.e., modules with known position). Among available techniques, the time of arrival (ToA) methods [1], [2], such as one-way ranging (OWR) [3] and two-way ranging (TWR) [4], do not require time synchronization between the anchor modules, while the time difference of arrival (TDoA) technique needs the clocks of the anchors to be synchronized [5], [6]. Although the same UWB hardware can be utilized to implement both ToA and TDoA, the latter solution requires an external computation module and an additional wireless network for performing the time synchronization between the anchors, thus increasing the cost and complexity of the TDoA methods. Among these options, the double-sided TWR-ToA technique presents a reasonable compromise, considering its accuracy and complexity [7]–[9], [19], and it is the method adopted in the current research.

Although many researchers in the last two decades focused on the design of the UWB-based indoor 2D and 3D position estimation methods and improving their performance ([29]–[32]), only a few investigations have been conducted on *velocity* estimation of a UAV in indoor environments. Alongside the position and attitude, velocity is one of the key states required to be estimated for any mobile robot in order to achieve autonomous guidance and navigation [10]. Frequently, motion capture (MoCAP) systems comprised of multiple cameras are used for absolute position and attitude estimation in an indoor environment. Since the MoCAP system provides highly accurate measurements at high rate (> 100Hz), one can use the first time-derivative of the estimated position signal to generate the absolute velocity of the UAV. However, MoCAP systems are expensive and more importantly, not available outside of research laboratories.

It has previously been shown that fusing the position estimation data and the acceleration measurement using Kalman or particle filters can lead to an estimation of velocity [11], [12]. The accuracy of the estimated velocity with these methods depends on the noise characteristics of the acceleration measurement. High variances and the presence of biases in the acceleration measurements, as typically observed on quadrotors with multiple rotating propellers, significantly degrade the accuracy of the velocity estimation. In [13], lateral drag forces are incorporated to propose a special extended Kalman filter for estimating the lateral attitudes, (i.e. pitch and roll angles) as well as the horizontal velocity components of a quadrotor. The algorithm needs the measurements of angular velocity of the quadrotor as well as the acceleration vector in the horizontal plane. Moreover, the robot mass and the constant coefficients of the lateral drag forces are required by the algorithm. In [14], a second-order sliding-mode differentiator is utilized for estimating the vertical velocity of a quadrotor, by fusing the acceleration measurements and the vertical position estimated with the OptiTrack MoCAP system.

There are some solutions in literature proposed for velocity estimation of mobile robots, which are not based on the

acceleration measurements. In quadrotors, having flexible blades and different blade tip speeds on a rotor provide a slight difference in the generated lift forces on the blades. This leads to a relative flapping up on the advancing blade and a relative pushing down on the retreating blade. This behavior on the blade-driven flying robots is referred to as *blade flapping*. It was shown that by incorporating the induced drag force from blade flapping in the dynamics equations of the quadrotor, an observer can be developed for estimating the horizontal velocity of the quadrotor in its body frame [10]. In [15], a solution based only on the blade flapping concept is suggested for estimating the body-frame velocity of a quadrotor. The algorithm requires information on mass of the robot as well as the parameters for characterizing the propeller thrust, and also measurements of the rotational speed of each motor. Thus, it is not a generic solution that can be implemented on any quadrotor, conveniently. Furthermore, additional experiments need to be conducted to provide the required information on the propellers.

An optical flow sensor provides an excellent alternative for estimating the velocity of an aerial mobile robot [16], [17]. In this sensor, the rate of change of the features captured by a camera (often mounted looking downwards on the quadrotor) is computed in the horizontal plane and then multiplied by the measured range to the features (computed by a sonar range finder) to estimate the 2D velocity of the quadrotor in its body frame. The attitude of the drone is utilized to convert the measured velocity to the inertial frame. However, the accuracy of the velocity estimation by the optical flow sensor strongly depends on the density and texture of features visible to the sensor. This is usually problematic for indoor environments since floors and walls tend to be plain and devoid of any texture. Recently, a solution was proposed in [18] that combines the lateral dynamics model of the quadrotor, the angular velocity and acceleration, the magnetometer and the estimated velocity from an optical flow sensor, to provide a clean estimation of the velocity in the body frame. This solution, however, is quite complicated and requires information on the lateral dynamics of the vehicle as well as its mass. In [19], a UWB-based position and velocity estimation solution (with TWR-ToA as the ranging method) is proposed and tested for a drone flying in horizontal plane, while no experimental results are reported to assess performance in the vertical (z-) axis. In that solution, a trilateration method with Newton algorithm as the optimization method, is utilized for initializing the estimation solution. Then, an extended Kalman filter (EKF) is proposed for estimating the position and velocity of the drone. This EKF requires a 3D acceleration measurement of the drone, which is replaced with a white noise signal.

In light of the above limitations, in this paper, a solution for velocity estimation of a quadrotor in inertial frame is provided based on the UWB signals. Although it requires the installation of anchors of the UWB system in the environment where the robot is flying, this solution is relatively simple and cheap. In our implementation of the UWB system, the ranging measurement from the tag module to each anchor is provided using ToA of transmitted signals. Thus, no time synchronization is required between the anchors, as the tag module is the initiator of the TWR measurement with all the anchors in a predefined order. Moreover, here it is assumed that all anchors are fixed in the environment and their positions are already known. The problem of moving anchors can be addressed in the framework of *cooperative localization* solutions [20]–[24], and is out of the scope of this paper. In addition, since all the ranging data are gathered and then processed for position and velocity estimations on-board the drone, there is no need for a ground station to perform the computations and to send the estimated states back to the drone. This makes the proposed solution inexpensive, independent of the communication link between the drone and the ground station and, convenient to install and transport. Moreover, the proposed solution does not require any information on the dynamics of the robot, nor does it depend on the noisy acceleration measurements. Specifically, the contributions of the paper are as follows:

- we provide a velocity estimation solution based on UWB signals, without requiring acceleration measurements nor dynamics model;
- the full linear state estimation (position and velocity) is implemented on-board the robot and is therefore independent of the ground station. Moreover, the estimated states are utilized for position control of a quadrotor, demonstrating indoor autonomous target tracking.

II. UWB-BASED VELOCITY ESTIMATION SOLUTION

Definition-1. The UWB system is defined as a system including n UWB anchors (where $n \geq 4$) and at-least one UWB tag module. In the system, each tag initiates the double-sided TWR process with each of the UWB anchors in a predefined order, and the anchors reply to the received request. We introduce a local frame of the UWB system, which has a local origin in the working environment. The positions of all UWB anchors are determined in this local frame and the estimated position of the UWB tag module is provided within the same local frame. For a UWB tag, its estimated position is transformed to the local NED frame by rotating through the yaw angle of the local UWB frame in the NED frame. The origin of the local NED frame is set to be at the origin of the local UWB frame. It is noted that the specific configuration of fixed anchors in the environment can affect the performance of the proposed position/estimation solution. Generally, the anchors should not be too close to each other and they should not lie in the same plane. A thorough analysis of anchor configuration and their optimization is presented in [25], [30].

Definition-2. The localization problem in a 3D environment with multiple anchors can be formulated as an optimization problem and we employ the gradient descent

(GD) method to solve it. In this regard, a representation is considered for the problem, by defining the closest anchor to the tag module as the reference point and subtracting the corresponding range measurement from the range measurements of other anchors [19]. Thus, the localization problem is stated as

$$\underset{\hat{\mathbf{p}}}{\text{minimize}} \ (\frac{1}{2}\mathbf{e_p}^T\mathbf{W_p}\mathbf{e_p}) \ , \tag{1}$$

where $\hat{\mathbf{p}} = [\hat{x}, \hat{y}, \hat{z}]^T \in \mathbb{R}^3$ is the estimated 3D position of the tag module and $\mathbf{W_p} \in \mathbb{R}^{m\times m}$ (for $m = n-1$) is a weight matrix for the measurements (defined in *Remark-2*). In addition, we define

$$\mathbf{e_p} = (\mathbf{B_p} - \hat{\mathbf{B}}_\mathbf{p}) \ \in \mathbb{R}^{m\times 1}, \tag{2}$$

where

$$\hat{\mathbf{B}}_\mathbf{p} = \mathbf{A_p}\hat{\mathbf{p}} \ , \tag{3}$$

in which

$$\mathbf{A_p} = \begin{bmatrix} 2(x_1 - x_r) & 2(y_1 - y_r) & 2(z_1 - z_r) \\ 2(x_2 - x_r) & 2(y_2 - y_r) & 2(z_2 - z_r) \\ 2(x_3 - x_r) & 2(y_3 - y_r) & 2(z_3 - z_r) \\ \vdots & \vdots & \vdots \\ 2(x_m - x_r) & 2(y_m - y_r) & 2(z_m - z_r) \end{bmatrix} \in \mathbb{R}^{m\times 3} \ ; \tag{4}$$

and

$$\mathbf{B_p} = \begin{bmatrix} (d_r^2 - x_r^2 - y_r^2 - z_r^2) - (d_1^2 - x_1^2 - y_1^2 - z_1^2) \\ (d_r^2 - x_r^2 - y_r^2 - z_r^2) - (d_2^2 - x_2^2 - y_2^2 - z_2^2) \\ (d_r^2 - x_r^2 - y_r^2 - z_r^2) - (d_3^2 - x_3^2 - y_3^2 - z_3^2) \\ \vdots \\ (d_r^2 - x_r^2 - y_r^2 - z_r^2) - (d_m^2 - x_m^2 - y_m^2 - z_m^2) \end{bmatrix} . \tag{5}$$

Note that here $\mathbf{p_i} = [x_i, y_i, z_i]^T$ is the position vector of the ith anchor in the local UWB frame and $d_i \in \mathbb{R}^+$ is the measured distance of the tag module to the ith anchor. Moreover, $r \in \{1, ..., n\}$ is the index of the reference anchor.

Lemma-1. By utilizing the GD method to solve the optimization problem defined in *Definition-2*, the position of the tag module in $3D$ space is updated iteratively at each time-step, using

$$\dot{\hat{\mathbf{p}}} = \boldsymbol{\alpha_p}\mathbf{A_p}^T\mathbf{W_p}\mathbf{e_p} \ , \tag{6}$$

with an initial solution $\hat{\mathbf{p}}_\mathbf{0} = [0, 0, 0]^T$. Here, $\boldsymbol{\alpha_p}$ is a diagonal positive definite matrix defined in $\mathbb{R}^{3\times 3}$ and includes the learning rates of GD algorithm along the three axes. Note that in each iteration of the optimization process, the values of $\hat{\mathbf{B}}_\mathbf{p}$ are determined by utilizing (3).

Remark-1. The choice of the reference anchor affects the accuracy and the consistency of the localization results. Here, the nearest anchor to the tag is considered as the reference anchor; it therefore changes as the tag module moves in the environment.

Remark-2. Here, the weight matrix for measurements, $\mathbf{W_p}$, is a diagonal positive-definite matrix where for $i \in [1, n] - \{r\}$, we define

$$\mathbf{W_p}(i, i) = \frac{d_s - d_i}{d_s} \ , \tag{7}$$

where $d_s = \max\{d_i\} + \delta_0$. The parameter $\delta_0 \in \mathbb{R}^+$ is used to avoid a zero value for the diagonal element of $\mathbf{W_p}$ corresponding to the highest measured distance.

Definition-3. Recalling the estimated 3D position of the UWB tag using *Lemma-1*, the Euclidean distance of the tag to the ith anchor can be written as follows (for $i \in [1, n]$)

$$(\hat{x}(t)-x_i)^2+(\hat{y}(t)-y_i)^2+(\hat{z}(t)-z_i)^2 = d_i(t)^2+\delta_i(t) \ , \tag{8}$$

where $\delta_i(t) \in \mathbb{R}$ is the error associated with the estimation process at time t. Differentiating (8) w.r.t. time, we obtain

$$\dot{\hat{x}}(t)(\hat{x}(t) - x_i) + \dot{\hat{y}}(t)(\hat{y}(t) - y_i) + \dot{\hat{z}}(t)(\hat{z}(t) - z_i) = \dot{d}_i(t)d_i(t) + \frac{1}{2}\dot{\delta}_i(t) \ . \tag{9}$$

Furthermore, we consider $\dot{\hat{\mathbf{p}}}(t) = [\dot{\hat{x}}, \dot{\hat{y}}, \dot{\hat{z}}] = [\hat{\dot{x}}, \hat{\dot{y}}, \hat{\dot{z}}] = \hat{\mathbf{v}}(t)$, where $\hat{\mathbf{v}}(t) \in \mathbb{R}^3$ is the estimated absolute 3D velocity of the UWB tag in the local frame of UWB system at time t. Assembling the multipliers on the left-hand side of the equation (9) for all of the anchors $i \in \{1, ..., n\}$, one obtains

$$\mathbf{A_v} = \begin{bmatrix} (\hat{x} - x_1) & (\hat{y} - y_1) & (\hat{z} - z_1) \\ (\hat{x} - x_2) & (\hat{y} - y_2) & (\hat{z} - z_2) \\ (\hat{x} - x_3) & (\hat{y} - y_3) & (\hat{z} - z_3) \\ \vdots & \vdots & \vdots \\ (\hat{x} - x_n) & (\hat{y} - y_n) & (\hat{z} - z_n) \end{bmatrix} \in \mathbb{R}^{n\times 3} \ . \tag{10}$$

Furthermore, the optimization problem for velocity estimation is defined as follows

$$\underset{\hat{\mathbf{v}}}{\text{minimize}} \ (\frac{1}{2}\mathbf{e_v}^T\mathbf{W_v}\mathbf{e_v}) \ , \tag{11}$$

where $\mathbf{W_v} \in \mathbb{R}^{n\times n}$ is a weight matrix for the measurements and its elements on the main diagonal are defined as in (7). In addition, we define

$$\mathbf{e_v} = (\mathbf{B_v} - \hat{\mathbf{B}}_\mathbf{v}) \in \mathbb{R}^{n\times n} \ , \tag{12}$$

in which

$$\hat{\mathbf{B}}_\mathbf{v} = \mathbf{A_v}\hat{\mathbf{v}} \ , \tag{13}$$

and

$$\mathbf{B_v} = \begin{bmatrix} \dot{d}_1 d_1 + \frac{1}{2}\dot{\delta}_1 \\ \dot{d}_2 d_2 + \frac{1}{2}\dot{\delta}_2 \\ \dot{d}_3 d_3 + \frac{1}{2}\dot{\delta}_3 \\ \vdots \\ \dot{d}_n d_n + \frac{1}{2}\dot{\delta}_n \end{bmatrix} \in \mathbb{R}^{n\times 1} \ . \tag{14}$$

Lemma-2. The same GD method is used to solve the velocity estimation problem in *Definition-3*, as for the position estimation problem. Hence, the velocity of the tag module in $3D$ space is updated iteratively at each time-step, using

$$\dot{\hat{\mathbf{v}}} = \boldsymbol{\alpha_v}\mathbf{A_v}^T\mathbf{W_v}\mathbf{e_v} \ , \tag{15}$$

with the initial solution of $\hat{\mathbf{v}}_\mathbf{0} = [0, 0, 0]^T$. Here, $\boldsymbol{\alpha_v} \in \mathbb{R}^{3\times3}$ includes the learning rates of the GD algorithm for velocity estimation along the three axes.

Remark-3. As can be seen from the right-hand side of (9), the time-derivatives of the estimated distances from the tag to all of the anchors as well as the associated estimation errors (i.e., δ_i) are required for the proposed velocity estimation algorithm. To deal with this issue, a sliding-mode differentiator is utilized following the work in [10], [27], [28]. For a generic scalar variable $h \in \mathbb{R}$, its time-derivative can be computed as

$$\dot{h} = \nu \,, \tag{16}$$

where

$$\begin{aligned} \dot{q} &= \nu \\ \nu &= -k_1 |q - h|^{1/2}\, sgn(q - h) + \nu_1 \\ \dot{\nu}_1 &= -k_2\, sgn(q - h) \end{aligned} \tag{17}$$

with $k_1 > 0$ and $k_2 > 0$ two constant parameters and $sgn(.)$ as the signum function [26].

Lemma-3. In the initial experiments with the proposed position and velocity estimation solutions, it was observed that there is noise on range measurements to the anchors and also in the z-axis position estimate. Consequently, two KFs are proposed for removing the noise on the range measurements (KF-1), as well as noise on the vertical position estimate (KF-2). The linear KF formulation is chosen, since the measurement models for the two aforementioned variables are linear. Each of the range measurements is computed by multiplying the measured time of flight of the corresponding RF signal by the speed of light. Also, the z-axis position estimation is formulated within a set of linear equations in (3). Hence, the motion and measurement models for the filters are formulated as follows:

$$\begin{aligned} \dot{\mathbf{x}} &= \mathbf{A_k x} \,, \\ w &= \mathbf{C_k x} \,, \end{aligned} \tag{18}$$

where

$$\mathbf{A_k} = \begin{bmatrix} 0 & 1 & 0 \\ 0 & 0 & 1 \\ 0 & 0 & 0 \end{bmatrix}, \quad \mathbf{C_k} = \begin{bmatrix} 1 & 0 & 0 \end{bmatrix}, \tag{19}$$

and $\mathbf{x} = [d_i; \dot{d}_i; \ddot{d}_i]$ $(i \in [1, n])$ for KF-1, while $\mathbf{x} = [z_t; \dot{z}_t; \ddot{z}_t]$ for KF-2. In (18), w is the corresponding measured distance or z-axis estimated position. It is assumed the measurements/estimations have constant second-derivatives. The complete workflow of the solution including the two Kalman filters is depicted in Fig. 1.

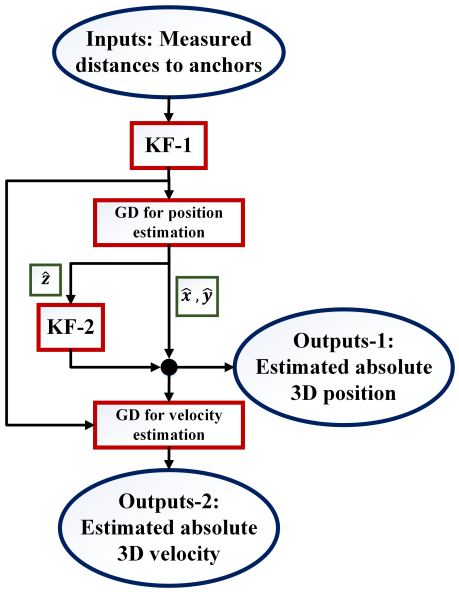

Fig. 1: 3D position and velocity estimation solution workflow based on UWB technologies.

III. Experimental set-up

A. The quadrotor

The experimental test results presented in this manuscript were carried out with a custom built small quadrotor ($\approx 300g$) with the following attached modules (Fig. 2):

- *Nanopi* board, for performing the proposed position/velocity estimation solution on-board, as well as the high-level position/velocity control of the quadrotor, running at 30Hz; here, the tuning parameters of the solution are set as $\boldsymbol{\alpha_p} = 1e\text{-}9\ \text{diag}([2, 2, 1])$, $\boldsymbol{\alpha_v} = 1e\text{-}8\ \text{diag}([1, 1, 1])$, $k_1 = 10.0$, $k_2 = 1.0$, $\delta_0 = 1000mm$.
- *pixracer* board, for handling the low-level attitude control of the quadrotor using the PX4 autopilot at 100Hz;
- *DWM1001-dev* module as the UWB tag for performing range measurements; it gathers data at 20-30Hz, depending on the number of available UWB anchors.
- To obtain ground-truth measurements with Vicon MoCap system, a rigid body with four markers is added on top of the quadrotor.

The communication between the Nanopi board and the pixracer board is implemented using the UART serial protocol. Similarly, the communication between the Nanopi board and the DWM1001-dev module is provided using UART. The off-set along z-axis of the vehicle between the location of the UWB tag and the centroid of the Vicon markers on the quadrotor is compensated in the results.

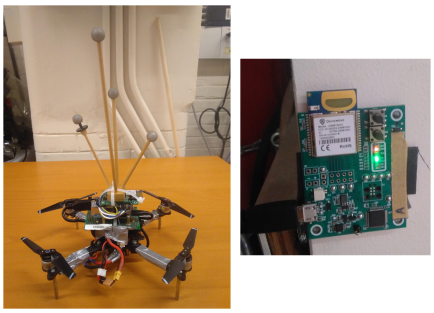

Fig. 2: Left: the quadrotor used for experiments. Markers are added for comparison with Vicon MoCap system. Right: a UWB anchor.

B. The UWB system

Here, a UWB system comprised of 8 anchors (see Fig. 2) is utilized for conducting the three test scenarios. Scenario-1 and scenario-3 are conducted at Space-1[1] with the approximate dimensions of $6m \times 6m \times 2.5m$, while Scenario-2 is organized in Space-2[2] with the approximate dimensions of $6m \times 6m \times 4m$, where Vicon MoCap system is available. The UWB system can be installed/uninstalled in either of the spaces conveniently (≈30 minutes), attesting to transportability of the system. The Vicon MoCap system has a dedicated ground station for processing the captured data from six cameras which are mounted on the ceiling, and generating the position/orientation of the quadrotor. In both spaces used for our experiments, the anchors are located at the vertices of a cube (see Fig. 3) and the quadrotor is flown within this cube during the experiments. Locations of the anchors can be optimized, using a recently proposed method [30], but this was not done here. The anchor locations in the two spaces are presented in Table I and Table II. Their positions were measured using a measuring tape, to within 1cm accuracy.

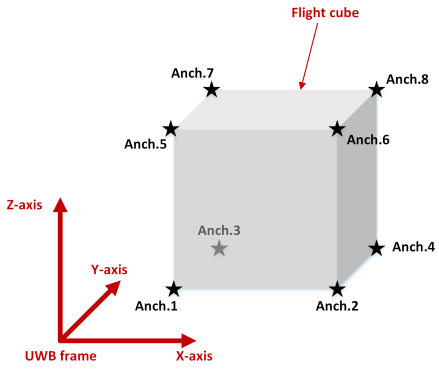

Fig. 3: The UWB system, the UWB frame and the flight cube.

TABLE I: Positions of anchors in UWB frame for experiments of scenario-1 and scenario-3 in Space-1

No.	Position (mm)	No.	Position (mm)
1	$[-500, 0, 250]$	2	$[4880, 0, 250]$
3	$[0, 5920, 280]$	4	$[5590, 5790, 400]$
5	$[0, 0, 2290]$	6	$[4880, 0, 2240]$
7	$[0, 5920, 2390]$	8	$[5260, 5790, 2290]$

TABLE II: Positions of anchors in UWB frame for experiment of scenario-2 in Space-2

No.	Position (mm)	No.	Position (mm)
1	$[1050, 1000, 1000]$	2	$[-1300, 3100, 1000]$
3	$[-5700, -2850, 1000]$	4	$[-5700, 2800, 1000]$
5	$[1050, 1000, 2500]$	6	$[-1300, 3100, 2500]$
7	$[-5700, -2850, 2500]$	8	$[-5700, 2800, 2500]$

[1]HumanITAS Solutions office, Montreal, QC, Canada
[2]AML, McGill University, Montreal, QC, Canada

IV. Experimental results

A. Scenario-1: Evaluation of Kalman filters

In this subsection, the use of two linear KFs proposed in *Lemma-3* is evaluated. In this regard, a set of manual flights of the drone is performed to collect the data for the $3D$ position estimation. The evaluation is conducted through a comparative study by including three different cases as follows:

- *Case-1*: The GD algorithms are used without filtering.
- *Case-2*: The GD algorithms are used with KF-2 only.
- *Case-3*: The GD algorithms are used with both filters KF-1 and KF-2.

Results for z-axis position (height) estimation, comparing the above three cases are provided in Fig. 4. As mentioned earlier, the results are logged during a manual flight of the drone in the 3D environment. In that flight, the altitude of the drone was maintained approximately constant at ≈20cm above floor level, while the drone was flown in the horizontal plane. Case-3 result shows an initial convergence phase introduced by filtering the range measurements to the 8 anchors. As can be seen in Fig. 4, the usage of both KF-1 and KF-2 at the same time, contributes to achieving a smoother position estimation along z-axis.

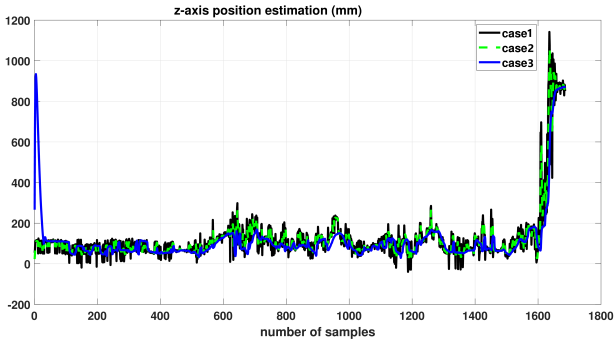

Fig. 4: Estimated z-axis position in three cases. Effect of using two KFs is visible in smoothing the estimate.

B. Scenario-2: Comparison with Vicon MoCap system

In order to evaluate the performance of our UWB-based position/velocity estimation solution, we employ a Vicon MoCap system as the ground-truth. The frequency of position estimation on the Vicon MoCap system is about 70Hz, while the proposed UWB position/velocity estimation tool is providing data at ≈30Hz. The velocity estimate for Vicon MoCap system is computed by using the sliding-mode differentiator in (17) on the estimated position data. Comparison of the results from the proposed UWB-based solution and Vicon Mocap system is provided in Figs. 5 and 6. Also, the corresponding mean values for the estimation errors are summarized in Table III. It is observed that the position and velocity components in the horizontal plane as estimated from the two measurement systems, are following each other

closely. The mean value of position estimation error in the horizontal plane is 180mm and for the velocity estimation, it is 78mm/s. The corresponding mean error values for the z-axis are slightly higher, especially for the velocity estimation. The ranging measurement noise, as well as the estimation errors in horizontal plane contribute to higher errors in z-axis position and velocity estimates. Similar performance for the vertical position (not velocity) estimation has been reported in [29].

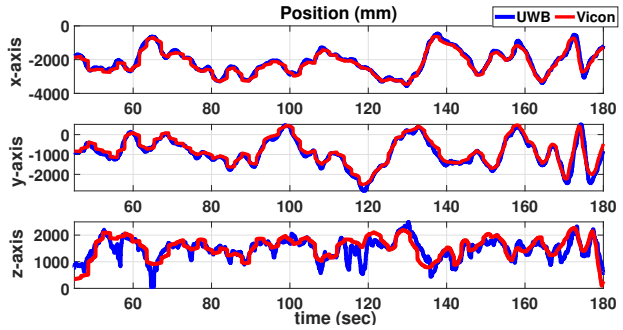

Fig. 5: Comparison of UWB 3D position estimation with Vicon MoCap system.

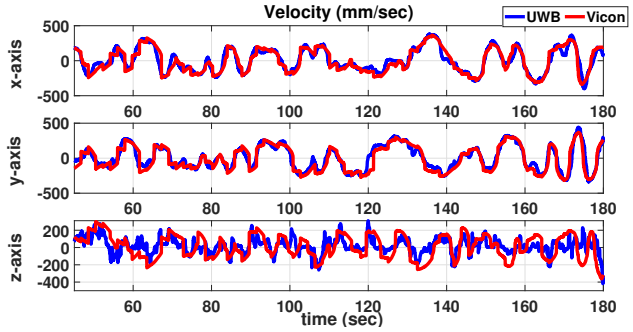

Fig. 6: Comparison of UWB 3D velocity estimation with Vicon MoCap system.

TABLE III: Comparison of UWB system with Vicon MoCap system: mean absolute errors for position/velocity estimates

Estimation error	Mean value	Estimation error	Mean value
x-axis position	116 mm	x-axis velocity	55 mm/s
y-axis position	138 mm	y-axis velocity	56 mm/s
z-axis position	235 mm	z-axis velocity	90 mm/s

C. Scenario-3: Quadrotor autonomous flight

Here, the results from a test with autonomous flight of the quadrotor using the proposed UWB position/velocity estimation solution are provided. It is emphasized that the goal of this scenario is not to demonstrate any particular controller, but to show the feasibility of closing the loop with the proposed UWB-based position/velocity estimation solution and achieving reasonable performance for the entire closed-loop system. In this regard, two sets of consecutive PID controllers have been implemented for position and velocity regulation of the drone in 3D space. The frequency of these controllers is set to 30Hz, aligned with the frequency of position/velocity estimation. The desired attitude set-points generated by PID position/velocity controllers are sent to the pixracer on the drone via a MAVLink message. Thus, the attitude controller within the PX4 platform is utilized for determining the desired set-points for the rotational speed of each propeller on the drone. In this test, a desired reference point at $(+3, -2, -0.5)$m in the local NED frame is requested after switching the drone to autonomous flight mode at $t = 20$s. The objective is to allow the drone to reach and hover at the desired set-point. The gains for the PID controllers are tuned by trial-and-error during lots of test flights. The results of this experiment are presented in Fig. 7 to Fig. 10. They confirm that the estimated position and velocity from the proposed UWB-based solution can be combined with a simple closed-loop controller for autonomous flight of the quadrotor in an indoor area. The fluctuations in the tracking errors for the position and velocity of the quadrotor are commensurate with the expected performance in light of the results in Section IV-B, taking into account disturbances on the vehicle and limitations of the controller.

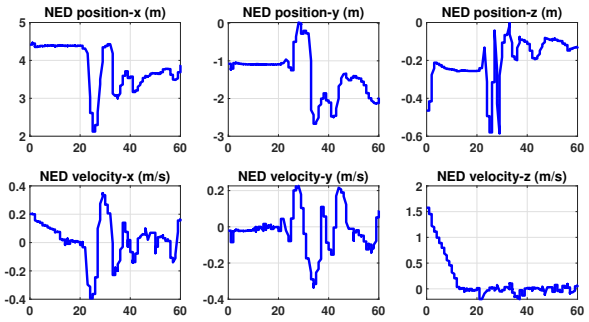

Fig. 7: 3D estimated position/velocity of drone in NED frame. Conversion from UWB frame to NED frame is accomplished by a rotation around z-axis through 35°.

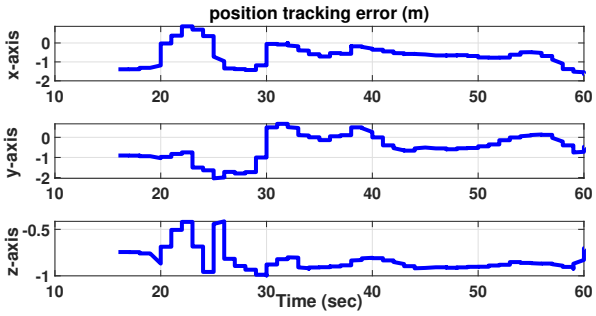

Fig. 8: Position tracking error in NED frame.

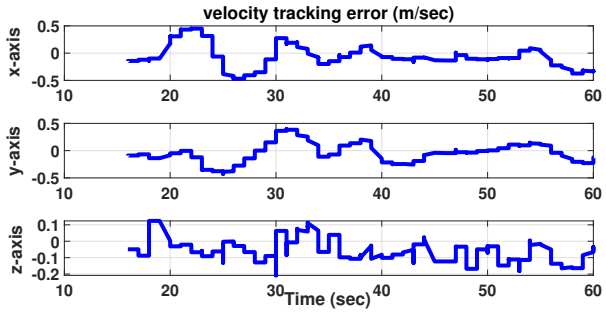

Fig. 9: Velocity tracking error in NED frame.

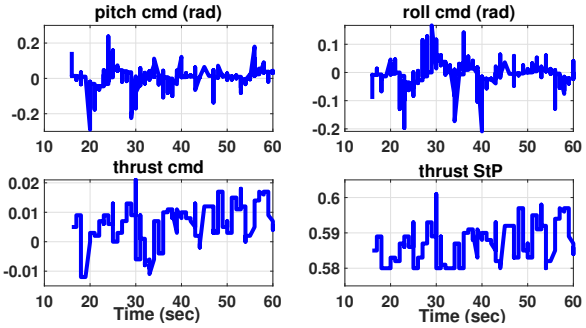

Fig. 10: Attitude set-points for the drone in NED frame. These values are sent to PX4 autopilot. The thrust set-point (i.e. thrust StP) has a constant term for gravity compensation, in addition to the commanded thrust force (i.e. thrust cmd).

V. Conclusion

In this paper, a solution for the velocity estimation of unmanned aerial vehicles in indoor areas is presented. The solution is based on UWB ranging measurements. It includes two gradient descent optimizations for 3D position and velocity estimations based on the ranging measurements received from multiple fixed anchors. Moreover, two linear Kalman filters are incorporated for removing the noise on the ranging measurements as well as on the z-axis position estimate. The solution is verified in three experimental scenarios. First, it is shown that the use of Kalman filters produces a significant smoothing of the estimates. Then, the accuracy of the proposed velocity estimation solution is evaluated in a 3D environment by comparing with the results from a Vicon MoCap system. It is observed that the velocity estimated data have a mean error of 78mm/s in the horizontal plane, while the mean accuracy of 90mm/s is achieved in the vertical direction. Finally, an autonomous flight of a quadrotor in indoor area is achieved by using the proposed position/velocity estimation solution. The UWB-based estimation solution presented in this paper can be used both in indoor and outdoor environments, where the anchors can be installed in known locations. In the future, more experiments should be conducted to identify the minimum number of anchors required to achieve convergence of the estimation errors to a desired tolerance. Moreover, it would be interesting to investigate options for merging the proposed UWB solution with vision-based odometry solutions, to exploit the advantages of both. Another suggestion is to use the VICON and UWB estimated position/velocity data to train a nonlinear model (e.g., a neural network) in order to fit a model to noise and errors of the UWB system. This fitted model could then be incorporated in the real-time position/velocity estimation with the UWB system in the field, to improve the accuracy of the estimation.

Acknowledgment

This research is conducted under a Mitacs Accelerate program at McGill University and HumanITAS Solutions. The authors want to thank Mr. Lam Son Vo Ngoc, from HumanITAS Solutions, for his help in conducting the tests for autonomous flights of the drone.

References

[1] Y.T. Chan, W.Y. Tsui, H.C. So and P.C. Ching, "Time-of-arrival based localization under NLOS conditions," *IEEE Transactions on Vehicular Technology*, vol. 55, no. 1, pp. 17-24, 2006.

[2] T.V. Haute, B. Verbeke, E.D. Poorter and I. Moerman, "Optimizing time-of-arrival localization solutions for challenging industrial environments," *IEEE Transactions on Industrial Informatics*, vol. 13, no. 3, pp. 1430-1439, 2017.

[3] H.S. Ahn, H. Hur and W.S. Choi, "One-way ranging technique for CSS-based indoor localization," in proc. of *6th IEEE Int. Conference on Industrial Informatics*, Daejeon, South Korea, pp. 1513-1518, 2008.

[4] M. Laaraiedh, S. Avrillon and B. Uguen, "Cramer-Rao lower bounds for nonhybrid and hybrid localization techniques in wireless networks," *Transactions on Emerging Telecommunications Technologies*, vol. 23, no. 3, pp. 268-280, 2012.

[5] C. Zhang, M. Kuhn, B. Merkl, A.E. Fathy and M. Mahfouz, "Accurate UWB indoor localization system utilizing time difference of arrival approach," in proc. of *2006 IEEE Radio and Wireless Symposium*, San Diego, CA, pp. 515-518, 2006.

[6] M.A. Landolsi, H.R. Khan, A.S. Al-Ahmari and A.H. Muqaibel, "On the performance of wireless sensor network time difference of arrival localization under realistic interference and timing estimation errors," *Int. Journal of Distributed Sensor Networks*, vol. 15, no. 2, 2019.

[7] D. Neirynck, E. Luk and M. McLaughlin, "An alternative double-sided two-way ranging method," in proc. of *13th Workshop on Positioning, Navigation and communications*, Bremen, Germany, pp. 1-4, 2016.

[8] K.A. Horvath, G. Ill and A. Milankovich, "Passive extended double-sided two-way ranging algorithm for UWB positioning," in proc. of *Ninth International Conference on Ubiquitous and Future Networks*, Milan, Italy, pp. 482-487, 2017.

[9] C.L. Sang, M. Adams, T. Hormann, M. Hesse, M. Porrmann and U. Ruckert, "An analytical study of time of flight error estimation in two-way ranging methods," in proc. of *2018 Int. Conference on Indoor Positioning and Indoor Navigation*, Nantes, France, pp. 1-8, 2018.

[10] A. Safaei, "Adaptive relative velocity estimation algorithm for autonomous mobile robots using the measurements on acceleration and relative distance," *Int. Journal of Adaptive Control and Signal Processing*, vol. 34, no. 3, pp. 372-388, 2020.

[11] J. Cui, S. Lai, X. Dong and B. Chen, "Autonomous navigation of UAV in foliage environment," *Journal of Intelligent and Robotic Systems: Theory and Application*, vol. 84, no. 1-4, pp. 259-276, 2016.

[12] D. Abeywardena, S. Kodagoda, G. Dissanayake and R. Munasinghe, "Improved state estimation in quadrotor MAVs: A novel drift-free velocity estimator," *IEEE Robotics and Automation Magazine*, vol. 20, no. 4, pp. 32-39, 2013.

[13] R.C. Leishman, J.C Jr. Macdonald, R.W. Beard and T.W. McLain, "Quadrotors and accelerrometers: state estimation with an improved dynamic model," *IEEE Control Systems Magazine*, vol. 34, no. 1, pp. 28-41, 2014.

[14] I. Boiko and M. Chehadeh, "Sliding-mode differentiator/observer for quadcopter velocity estimation through sensor fusion," *Int. Journal of Control*, vol. 91, no. 9, pp. 2113-2120, 2018.
[15] R. Mahony, V. Kumar and P. Corke, "Multirotor aerial vehicles: modeling, estimation and control of quadrotors," *IEEE Robotics and Automation Magazine*, vol. 19, no. 3, pp. 20-32, 2012.
[16] M. Saska, "MAV-swarms: unmanned aerial vehicles stabilized along a given path using onboard relative localization," in proc. of *Int. Conf. on Unmanned Aircraft Systems*, Denver, CO, pp. 894-903, 2016.
[17] K. Alexis, C. Papachristos, G. Nikolalopoulos and A. Tzes, "Model predictive quadrotor indoor position control," in proc. of *19th Med. Conf. on Control and Automation*, Corfu, Greece, pp. 1247-1252, 2011.
[18] D. Sartori, D. Zou, L. Pei and W. Yu, "A Revisited approach to lateral acceleration modeling for quadrotor UAVs state estimation," in proc. of *2018 IEEE/RSJ Int. Conference on Intelligent Robots and Systems*, Madrid, Spain, pp. 5711-5718, 2018.
[19] K. Guo, Z. Qiu, C. Miao, A.H. Zaini, C.-L. Chen, W. Meng and L. Xie, "Ultra-wideband-based localization for quadcopter navigation," *Unmanned Systems*, Vol. 4, No. 1, pp. 23-34, 2016.
[20] S. Safavi and U.A. Khan, "An opportunistic linear-convex algorithm for localization in mobile robot networks," *IEEE Transactions on Robotics*, vol. 33, no. 4, pp. 875-888, 2017.
[21] Z. Han, K. Guo, L. Xie and Z. Lin, "Integrated relative localization and leader-follower formation control," *IEEE Transactions on Automatic Control*, vol. 64, no. 1, pp. 20-34, 2019.
[22] A. Safaei and M.N. Mahyuddin, "Adaptive cooperative localization using relative position estimation for networked systems with minimum number of communication links," *IEEE Access*, vol. 7, pp. 32368 - 32382, 2019.
[23] C. Gao, G. Zhao, and H. Fourati, *Cooperative Localization and Navigation: Theory, Research, and Practice (1st ed.)*, CRC Press; 2019.
[24] T. -M. Nguyen, Z. Qiu, T. H. Nguyen, M. Cao and L. Xie, "Distance-Based Cooperative Relative Localization for Leader-Following Control of MAVs," *IEEE Robotics and Automation Letters*, vol. 4, no. 4, pp. 3641-3648, 2019. doi: 10.1109/LRA.2019.2926671.
[25] S. Monica and G. Ferrari, "Maximum likelihood optimization: when does it fail?", *ICT Express*, vol. 2, no. 1, pp. 10-13, 2016.
[26] A. Levant, "Robust exact differentiation via sliding mode technique," *Automatica*, vol. 34, no. 3, pp. 379-384, 1998.
[27] Safaei A. and M. N. Mahyuddin, "Optimal model-free control for a generic MIMO nonlinear system with application to autonomous mobile robots," *Int. Journal of Adaptive Control and Signal Processing*, Vol. 32, no. 6, pp. 792-815, 2018.
[28] Safaei A. and M. N. Mahyuddin, "Adaptive model-free control based on an ultra-local model with model-free parameter estimations for a generic SISO system," *IEEE Access*, Vol. 6, pp. 4266-4275, 2018.
[29] E. Fresk, K. Odmark and G. Nikolakopoulos, "Ultra wideband enabled inertial odometry for generic localization," *IFAC-PapersOnLine*, vol. 50, no. 1, pp. 11465-11472, 2017.
[30] W. Zhao, M. Vukosavljev and A. P. Schoellig, "Optimal Geometry for Ultra-wideband Localization using Bayesian Optimization," *IFAC-PapersOnLine*, vol. 53, no. 2, pp. 15481-15488, 2020.
[31] M. Hamer and R. D'Andrea, "Self-calibrating ultra-wideband network supporting multi-robot localization", *IEEE Access*, vol. 6, pp. 22292-22304, 2018.
[32] N. Balaji, M. Kothari and A. Abhishek, "GPS denied localization and magnetometer-free yaw estimation for multi-rotor UAVs," in proceedings of *International Conference on Unmanned Aircraft Systems (ICUAS)*, Athens, Greece, pp. 983-990, 2020